

Radiation dose assessment of ^7Be and activated corrosion products present in the hydrogen trap of IFMIF-DONES lithium system

J. Javier Martínez-Serrano^{a,*}, Yuefeng Qiu^b, Tamás Dézsi^c, Francesco Saverio Nitti^d, Angel Ibarra^e

^a Departamento de Física Aplicada I, Universidad de Málaga, Málaga, Spain

^b Karlsruhe Institute of Technology, KIT, Karlsruhe, Germany

^c Centre for Energy Research, Fusion Technology Department, / C3D Engineering Ltd., Budapest, Hungary

^d ENEA Brasimone, BO, Camugnano I-40032, Italy

^e Consorcio IFMIF-DONES España, Granada, Spain

ARTICLE INFO

Keywords:

Ambient dose equivalent rate

Hydrogen trap

^7Be

Activated corrosion product

IFMIF-DONES

ABSTRACT

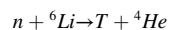
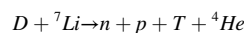
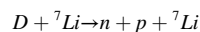
The radiological impact that ^7Be and activated corrosion products (ACP) dissolved in Li could have in normal operation and maintenance in the surroundings of the hydrogen trap (HT) of future IFMIF-DONES facility has been assessed. Ambient dose equivalent rates were calculated with radiation transport program MCNP at half height of trap. Four different Y contents were considered in the trap: 1, 3, 5 and 8 kg. In normal operation dose rates in the range 13.7–15.1 mSv/h have been found in contact with the trap and 0.28–0.31 mSv/h at 1 m of the trap. ^7Be has a very low contribution to dose (3–3.7 $\mu\text{Sv/h}$). Dose simulations have shown that a concrete wall 30 cm thick can reduce dose rates to acceptable dose limits. In maintenance operation the trap is drained and Li film remains attached to Y pebbles. Three possible Li film thickness have been considered: 10, 50 and 100 μm . Estimated ^7Be activity is below exemption limits during maintenance. Assessed dose rates are in the range 34–1420 $\mu\text{Sv/h}$ at contact with the trap and a maximum of 10.9 $\mu\text{Sv/h}$ at 1 m of the trap.

1. Introduction

In IFMIF-DONES, nuclear stripping reactions will occur at the target assembly (TA) where an accelerated deuteron beam of 40 MeV and 125 mA will collide with a liquid lithium target jet of 25 mm thick flowing at a nominal speed of around 15 m/s. These nuclear reactions have the objective of producing a neutron flux in the order of $1\text{--}5 \times 10^{14}$ n/cm²/s that will irradiate a set of material samples causing significant damage on them. The nuclear reactions are aiming to be continuously operated during sufficiently long periods of time and with a neutron environment similar to that expected in the first wall of a future fusion reactor.

Apart from the desired generation of large amount of high energy neutrons, the interactions between the deuteron beam and the lithium target will lead to the production of different impurities that will be dragged within the lithium flow (protium, deuterium and tritium). The major source of hydrogen impurities in the lithium flow is coming from the deuterium which is incorporated within the flow during the continuous process of injection and stopping of the deuteron beam into the lithium target.

In addition to the generation of deuterium inside the lithium flow, the uninterrupted production of protons and tritium is also considered, which is given basically by the following stripping reactions. For additional stripping reactions producing tritium see reference [1]:



The concentration of hydrogen isotopes on the loop should be carefully limited and bounded. There are two important reasons to perform the control of the hydrogen isotopes concentration: the first reason is related to the presence of tritium on the closed lithium loop that can lead to some radiological risks if the radioactive inventory and/or concentration exceed limited values. Second main reason is that a high concentration of these impurities could generate LiH precipitates that may provoke deleterious effects on the system as higher corrosion rates on

* Corresponding author.

E-mail address: jmserrano@uma.es (J.J. Martínez-Serrano).

<https://doi.org/10.1016/j.fusengdes.2024.114269>

Received 5 December 2023; Received in revised form 23 January 2024; Accepted 14 February 2024

Available online 17 February 2024

0920-3796/© 2024 The Authors. Published by Elsevier B.V. This is an open access article under the CC BY license (<http://creativecommons.org/licenses/by/4.0/>).

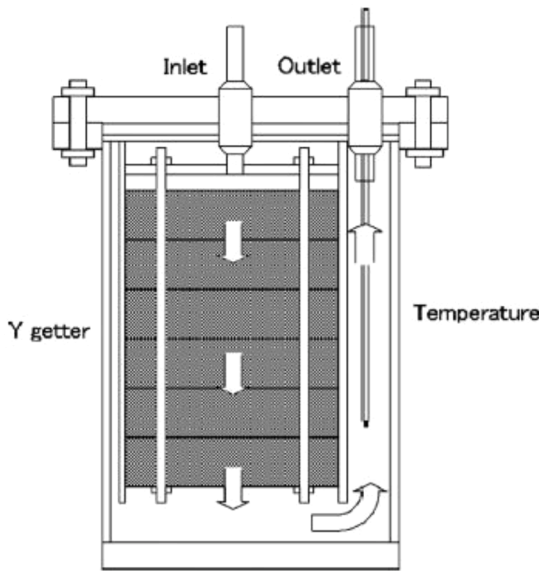


Fig. 1. Layout of the hydrogen hot trap [2].

the pipes and components that can affect to the performance and durability of the whole loop.

In addition to the hydrogen isotopes generated due to the presence of the deuteron beam impinging on the lithium loop, hydrogen is an ubiquitous impurity that will be also present on the stainless steel of the pipes and components of the loop. At the beginning of the operation, the presence of hydrogen coming from the physical elements that forms the loop will have an important contribution.

The concentration of the hydrogen isotopes in the lithium should be kept below specific limits by means of a system that captures the hydrogen. The capture system is based in an yttrium hydrogen trap (H-trap) which is part of a more general impurity control system where the H-trap is in line with a Cold Trap (CT), which is able to remove other impurities as the oxygen that is a poison for the yttrium. The basic configuration of the H-trap is a set of Y pebbles contained inside a stainless steel mesh crossed by the liquid lithium flow working at the same temperature as the whole loop.

The basic configuration of the Hydrogen trap is based on the proposal of Edao et al. [2]. Fig. 1 shows a scheme of the hydrogen trap. The main body trap holding the filter case is a cylinder of 60 cm length, 21.8 cm internal diameter and 2 mm thickness. A flange closes the main body at the upper side. A lower cover closes the main body at the lower part and has a hole so that it should be possible to drain the Li. The Y filter case is a metal cylinder of length 50 cm and radius 16 cm that contains spherical 1 mm Y pebbles. Thickness of the filter case is 1 mm. Maximum capacity of the filter is 22 kg of Y pebbles. Material of the filter is stainless steel SA 312 TP316L.

Over the generation of H-isotopes a radiological problem of concern is the presence in the Li loop of activation products. One of them is ⁷Be. A high amount of ⁷Be ($T_{1/2} = 53.3$ d) is generated in ^D-Li interactions, mainly by the reactions ⁶Li(D,n)⁷Be (14.5 %) and ⁷Li(D,2n)⁷Be (83.1 %). In addition a small quantity of the beta emitter ¹⁰Be is produced ($T_{1/2} = 1.6 \times 10^6$ y). ⁷Be decays in ⁷Li with gamma emission of 0.48 MeV. The production rate equilibrium value is around 150 mg, corresponding to 1.89×10^{15} Bq in 345 days of full operation. The plant stops 20 days a year for planned maintenance.

Moreover, activated corrosion products (ACP) are produced in the pipes walls and other components of the Li system by erosion and corrosion of flowing Li. These radionuclides are produced by activation of metal impurities when they move throughout the deuteron beam during the circulation of the Li in the target section. The ACPs can deposit in different parts of the Li system loop due to concentration

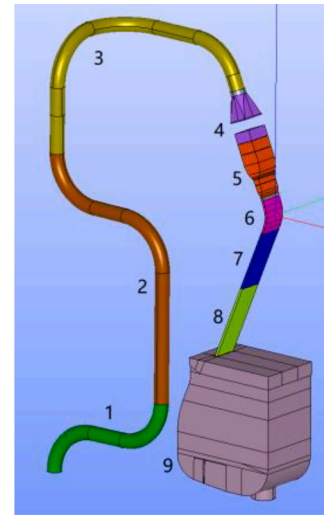


Fig. 2. Segments of the Li test cell.

Table 1

Dominant nuclei and parent nuclei by neutron activation in the segment 6.

Eurofer		SS316L	
Child	Parent	Child	Parent
⁵⁶ Mn	⁵⁶ Fe(n,p)98.3 %	⁵⁶ Mn	⁵⁵ Mn(n,g) 1.6 %
	⁵⁷ Fe(n,np) 1.22 %		⁵⁶ Fe(n,p) 96.9 %
⁵⁵ Fe	⁵⁶ Fe(n,2n) 99.3 %	⁵⁵ Fe	⁵⁷ Fe(n,np) 1.4 %
	Fe-54(n,g) 0.5 %		⁵⁶ Fe(n,2n) 95.0 %
⁵⁴ Mn	⁵⁵ Mn(n,2n) 3.8 %	⁵⁴ Mn	⁵⁸ Ni (n,a) 4.3 %
	⁵⁴ Fe(n,p) 64.6 %		⁵⁵ Mn (n,2n) 21 %
	⁵⁶ Fe(n,nd) 2.7 %		⁵⁴ Fe(n,p) 50.4 %
	⁵⁶ Fe(n,2np)26.5 %		⁵⁶ Fe(n,2np) 24.5 %
⁵¹ Cr	⁵⁶ Fe (n,t) 2.2 %	⁵¹ Cr	⁵⁸ Ni(n,pa) 3.7 %
	⁵² Cr(n,2n) 83.0 %		⁵² Cr(n,2n) 92.5 %
	⁵³ Cr(n,3n) 1.0 %		⁵⁴ Fe(n,a) 4.5 %
	⁵⁴ Fe (n,a) 11.5 %		
¹⁸¹ W	⁵⁶ Fe (n,2na) 3.6 %	⁵⁸ Co	⁵⁸ Ni (n,p) 99.2 %
	¹⁸² W(n,2n) 78.7 %		
	¹⁸³ W(n,3n) 15.1 %		
²⁸ Al	¹⁸³ W (n,4n)5.6 %	⁵⁷ Ni	⁵⁸ Ni(n,2n)100 %
	²⁸ Si(n,p) 96.7 %		⁵² Cr(n,p)89.2 %
	⁶⁰ Ni (n,p) 90.0 %		⁵³ Cr(n,np)5.6 %
	⁶³ Cu (n,a) 3.8 %		⁵³ Cr (n,d)1.1 %
⁶⁰ Co		⁵² V	⁵⁵ Mn (n,a)2.7 %

difference and local flow conditions. The H-trap can collect a significant amount of activated impurities due to the internal structure and the low velocity field of the flowing lithium.

In this paper we evaluate the radiological impact of ⁷Be and ACPs dissolved in Li in the H-trap, in order to justify the radiological classification of the H-trap cell, as well as evaluation on the shielding needs based on a parametric study of different Y contents in the H-trap. The main radioisotopes in ACP have been analyzed in the Section 2, with the contribution from deuteron and neutron activation in several locations. In Section 3, the amount of ACP and the resulting dose rates during operation and maintenance has been analyzed by parametric study of amount of Y pebbles.

2. Methods

The dominant ACPs considered in this study are: ²⁸Al, ⁵¹Cr, ⁵⁵Co, ⁵⁶Co, ⁵⁷Co, ⁵⁸Co, ⁶⁰Co, ^{60m}Co, ⁵⁵Fe, ⁵²Mn, ⁵⁴Mn, ⁵⁶Mn, ⁵⁷Ni, ⁵²V and ¹⁸¹W. In order to obtain the list of dominant radioisotopes and pathways, activation analyses of deuteron and neutron in segment 6 (Fig. 2)

Table 2
Dominant nuclei and parent nuclei by neutron activation in segment 7.

Eurofer		SS316L	
Child	Parent	Child	Parent
⁵⁶ Mn	⁵⁵ Mn(n,g) 8.e6 %	⁵⁶ Mn	⁵⁵ Mn(n,g) 40.3 %
	⁵⁶ Fe(n,p) 90.7 %		⁵⁶ Fe (n,p) 59.2 %
⁵⁵ Fe	⁵⁴ Fe (n,g) 7.0 %	⁵⁵ Fe	⁵⁴ Fe (n,g) 6.6 %
	⁵⁶ Fe (n,2n) 92.8 %		⁵⁶ Fe (n,2n) 86.6 %
⁵⁴ Mn	⁵⁴ Fe(n,p)87.8 %	⁵⁴ Mn	⁵⁹ Ni (n,a) 6.7 %
	⁵⁶ Fe(n,2np)7.6 %		⁵⁵ Mn (n,2n) 16.1 %
	⁵⁶ Fe (n,t) 0.98 %		⁵⁴ Fe (n,p) 73.9 %
	⁵⁵ Mn(n,2n)2.7 %		⁵⁶ Fe (n,nd) 0.6 %
⁶⁰ Co	⁵⁹ Co(n,g)55.3 %	⁶⁰ Co	⁵⁶ Fe (n,2np) 6.4 %
	⁵⁹ Co(n,g)44.2 %		⁵⁶ Fe (n,t) 0.8 %
²⁸ Al	²⁸ Si (n,p) 90.4 %	⁵⁸ Co	⁵⁹ Co(n,g) ^{60m} Co 30.6 %
	³¹ P (n,a) 1.3 %		⁵⁹ Co(n,g) 24.5 %
	⁵² Cr(n,p) 88.7 %		⁶⁰ Ni(n,p) 25.2 %
	⁵³ Cr (n,np) 2.9 %		⁶⁰ Ni(n,p) 16.7 %
⁵¹ Cr	⁵³ Cr (n,d) 0.61 %	⁵¹ Cr	⁶³ Cu (n,a) 1.7 %
	⁵⁵ Mn (n,a) 2.4 %		⁵⁸ Ni(n,p) 54.2 %
	⁵⁰ Cr(n,g) 13.4 %		⁵⁸ Ni(n,p) ^{58m} Co 44.8 %
⁵² V	⁵² Cr(n,p) 88.7 %	⁵² V	⁵⁰ Cr (n,g) 14.9 %
	⁵³ Cr (n,np) 2.9 %		⁵² Cr (n,2n) 78.5 %
	⁵³ Cr (n,d) 0.61 %		⁵⁴ Fe (n,a) 5.5 %
⁵¹ Cr	⁵⁵ Mn (n,a) 2.4 %	⁵¹ Cr	⁵² Cr (n,2n) 78.5 %
	⁵⁰ Cr(n,g) 13.4 %		⁵⁴ Fe (n,a) 5.5 %
	⁵² Cr(n,2n) 70.5 %		
⁵⁴ Mn	⁵⁴ Fe(n,a) 14.6 %	⁵⁴ Mn	

Table 3
Dominant nuclei and parent nuclei by deuteron activation in segment 6.

Eurofer		SS316L	
Child	Parent	Child	Parent
⁵⁶ Co	⁵⁶ Fe(d,2n) 73.3 %	⁵⁶ Co	⁵⁶ Fe(d,2n) 67.2 %
	⁵⁶ Fe(d,O) 26.7 %		⁵⁶ Fe(d,O) 24.5 %
⁵⁵ Fe	⁵⁶ Fe(d,nd) 2.7 %	⁵⁵ Fe	⁵⁸ Ni (d,O) 4.8 %
	⁵⁶ Fe(d,2np) 27.8 %		⁵⁶ Fe(d,2np) 26.8 %
	⁵⁶ Fe(d,O) 62.9 %		⁵⁶ Fe(d,O) 60.7 %
	⁵⁶ Fe(d,3n) ⁵⁵ Co 1.3 %		⁵⁶ Fe(d,3n) 1.3 %
	⁵⁶ Fe(d,O) ⁵⁵ Co 1.3 %		⁵⁶ Fe(d,O) 2.6 %
⁵¹ Cr	⁵² Cr(d,2np) 21.8 %	⁵¹ Cr	⁵⁶ Fe(d,3n) ⁵⁵ Co 1.3 %
	⁵² Cr (d,O) 40.0 %		⁵⁶ Fe(d,O) ⁵⁵ Co 2.6 %
	⁵² Cr(d,3n) ⁵¹ Mn 2.1 %		⁵² Cr(d,2np) 24.6 %
	⁵² Cr(d,O) ⁵¹ Mn 4.4 %		⁵² Cr (d,O) 54.3 %
⁵⁴ Mn	⁵⁶ Fe(d,O) 9.7 %	⁵⁴ Mn	⁵² Cr (d,3n) ⁵¹ Mn 2.4 %
	⁵⁶ Fe (d,a) 15.3 %		⁵² Cr((d,O) ⁵¹ Mn 5.0 %
	⁵⁶ Fe (d,O) 62.9 %		⁵⁶ Fe (d,O) 3.7 %
	⁵⁴ Fe (d,2p) 10.1 %		⁵⁶ Fe (d,a) 12.1 %
	⁵⁴ Fe (d,O) 4.4 %		⁵⁶ Fe (d,O) 49.9 % ⁵⁵ Mn(d,2np) 5.8 %
⁵² Mn	⁵⁵ Mn (d,2np)1.0 %	⁵² Mn	⁵⁵ Mn (d,O) 11.5 %
	⁵⁵ Mn (d,O) 2.0 %		⁵⁴ Fe(d,2p) 8.0 %
	⁵² Cr (d,O) 7.4 %		⁵⁴ Fe(d,O) 3.5 %
	⁵² Cr (d,2n) 24.8 %		
	⁵⁶ Fe (d,O) 46.4 %		
⁵⁵ Co	⁵⁶ Fe (d,2na) 8.66 %	⁵⁵ Co	⁵² Cr(d,O) 12.6 %
	Fe-54 (d,O) 6.6 %		⁵² Cr(d,2n) 42.5 %
	⁵⁶ Fe (d,3n)31.5 %		⁵⁶ Fe (d,O) 26.9 %
	⁵⁶ Fe (d,O) 63.5 %		⁵⁶ Fe (d,2na) 5.0 %
⁵² V	⁵⁴ Fe (d,n) 4.5 %	⁵² V	⁵⁴ Fe(d,O) 3.8 %
	Cr-52 (d,2p) 27.6 %		⁵⁸ Ni (d,O) ^{58m} Co 13.1 %
	Cr-52(d,O) 41.1 %		⁵⁸ Ni (d,2p) ^{58m} Co 42.2 %
⁵⁷ Co	Cr-53(d,O) 12.6 %	⁵⁷ Co	⁵⁸ Ni (d,O) 7.6 %
	Fe-56(d,O) 9.1 %		⁵⁸ Ni (d,2p) 18.9 %
	⁵⁶ Fe (d,n) 75.8 %		⁶⁰ Ni (d,O) ^{58m} Co 5.8 %
	⁵⁶ Fe (d,O) 6.4 %		
²⁸ Al	⁵⁷ Fe (d,2n) 12.5 %	⁶⁰ Co	⁵⁶ Fe (d,n) 23.1 %
	⁵⁷ Fe (d,O) 2.6 %		⁵⁸ Ni(d,n2p)18.5 %
			⁵⁸ Ni (d,O) 39.0 %
			⁵⁸ Ni (d,2np) ⁵⁷ Ni 1.2 %
⁵⁴ Mn		⁵⁴ Mn	⁵⁸ Ni (d,O) ⁵⁷ Ni 5.3 %
			⁶⁰ Ni(d,O) 21.6 %
			⁶⁰ Ni(d,2p) 34.0 %
			⁶⁰ Ni(d,O) ^{60m} Co 13.3 %
⁵¹ Cr		⁵¹ Cr	⁶⁰ Ni(d,2p) ^{60m} Co 15.6 %

Table 4
ACP mass content in the whole Li system.

Activation product	mass (mg)
⁵⁴ Mn	3.11 × 10 ⁻¹
⁵¹ Cr	2.53 × 10 ⁻⁵
⁵⁷ Co	1.18
⁶⁰ Co	6.28 × 10 ⁻²
^{60m} Co	1.57 × 10 ⁻⁶
⁵⁵ Co	9.46 × 10 ⁻⁵
⁵⁶ Co	1.29 × 10 ⁻¹
⁵⁸ Co	4.11 × 10 ⁻¹
⁵⁵ Fe	9.82 × 10 ⁻²
⁵² Mn	7.55 × 10 ⁻⁴
⁵⁶ Mn	7.88 × 10 ⁻⁵
⁵⁷ Ni	1.59 × 10 ⁻³
¹⁸¹ W	5.91 × 10 ⁻⁹
²⁸ Al	5.13 × 10 ⁻⁷
⁵² V	6.51 × 10 ⁻⁸

and neutron activation in segment 7 (Fig. 2) have been performed on both Eurofer and SS316L steel structural materials of the test cell (TC). The reason for choosing segment 7 for neutron activation calculation is that it represents other segments with neutron flux spectra in the TC environment, which have softer neutrons than that directly from the target in segment 6. TC segment 6 is exposed under the deuteron beam and the uncollided neutrons. Tables 1 and 2 shows neutron activation reactions in segment 6 and 7 respectively for the two steel types in the TC. Table 3 collects deuteron activation reactions for the two steel types. These dominant isotopes were evaluated through the irradiation of 1 cm³ Eurofer and SS316L under the neutron and deuteron fluxes using FISPACT-II code [3] with the activation cross section from TENDL-17 [4].

Neutron fluxes in different segments of the Li loop inside the TC were assessed in order to calculate the nuclear reaction rates. The average neutron flux spectra in 709 CCFE group [5] have been calculated in the Li volume using the reference TC neutronics model version mdl9.0.0, McDeLicious code [6], and FENDL3.1d [7] neutron cross sections. The deuteron flux is simulated using a similar approach used in [8].

The trap has been modelled as a simple cylinder of stainless steel SS316L (X2CrNiMo17–12–2) with dimensions: 59.6 cm inner height, 10 cm inner radius and 3 mm thickness (2 mm is the thickness of the main body trap and 1 mm is the Y filter case thickness [9]). Volume of the trap is 22 liters.

⁷Be is dissolved in Li as Be₃N₂. ⁷Be concentration inside the H-trap is assumed to be the same as at the exit of the cold trap. The concentration depends on temperature and N content. Temperature at the exit of cold trap is 190°C and N content is 10 wppm. Moreover, a 100% efficiency in the cold trap is assumed. Under mentioned conditions the ⁷Be concentration in Li is 1.0522 × 10⁻⁷ appm (obtained by equation 1 of [10]).

ACPs mass concentration in Li was obtained from a 1D convective mass transfer simulation of the Li loop (Table 4). The model calculates the mass transfer between the Li flow and the walls of the different components of the Li system based on local properties (temperature, materials of the components, corrosion rates, flow velocities, etc.). ACP transfer between the Li system wall components and the Li flow is governed by the concentration gradient between them. A convective term is considered for ACP transport along the Li loop. When ACPs reach the test cell they get irradiated. For the activation calculation, the ACP production rates have been computed for the Li segments corresponding to the local neutron and deuteron flux and Li volume.

Since the trapping is not modelled explicitly in the above mentioned 1D convective model next assumptions were considered to estimate ACP concentration in the H-trap: ACPs whose concentration is above the saturated value at CT temperature (190 °C) are completely trapped in the trap (⁵⁵Fe, ⁵¹Cr, ⁵⁷Co and ⁶⁰Co). ⁵⁴Mn does not saturate at loop

Table 5
Decay gamma energies and intensities of ⁷Be and ACPs.

Activation product	T _{1/2}	Energy (MeV)	Intensity
⁷ Be	53.22 d	0.477	0.1044
⁵⁴ Mn	312.08 d	0.835	0.9998
⁵¹ Cr	27.7 d	0.320	0.091
⁵⁵ Co	17.53 h	0.477	0.2018
		0.931	0.75
		1.317	0.0708
		1.370	0.0292
		1.408	0.1687
⁵⁷ Co	271.74 d	0.014	0.0916
		0.122	0.856
		0.136	0.1068
⁶⁰ Co	5.27 y	1.173	0.9985
		1.332	0.998
^{m60} Co	10.47 min	0.0586	0.02
⁵⁶ Co	77.24 d	0.847	0.999
		1.038	0.142
		1.238	0.669
		1.771	0.155
		2.598	0.173
		3.253	0.081
⁵⁸ Co	70.856 d	0.811	0.9945
⁵⁵ Fe	2.756 y	0.005888	0.0846
		0.005899	0.1659
		0.006490	0.034
⁵² Mn	5.59 d	0.744233	0.9
		0.935	0.945
		1.246	0.042
		1.333	0.051
		1.434	1
⁵⁶ Mn	2.58 h	0.847	0.9887
		1.811	0.272
		2.113	0.143
⁵⁷ Ni	35.6 h	0.127	0.167
		0.138	0.817
		0.176	0.0575
		0.192	0.122
¹⁸¹ W	120.96 d	0.00624	0.0103
		0.152	0.00083
²⁸ Al	2.24 min	1.779	1
⁵² V	3.74 min	1.334	0.0059
		1.434	1
		1.531	0.0012

temperature, hence the CT does not reduce its concentration. Therefore, assumed ⁵⁴Mn concentration in the H-trap is the average value in the loop considering this radionuclide is homogeneously distributed along the loop. ACP mass contents in the H-trap were assessed using the ACP masses in the whole Li system (Table 4), the Li volume in the H-trap and the total Li volume in the system (8.83 m³ [11]).

Dose assessment was carried out in normal operation and in maintenance. In normal operation a parametric study on Y mass was carried out. Four different Y contents were considered in the H-trap: 1, 3, 5 and 8 kg.

In maintenance all the Li in the H-trap is drained but a thin film remains attached to the Y pebbles. A parametric study based on Li film thickness attached to Y pebbles and the four Y mass contents mentioned before was carried out. Three different Li thickness were considered: 10, 50 and 100 μm. The Li mass attached to the spherical Y pebbles was estimated from the number of Y pebbles, the surface area of a pebble, the Li layer thickness attached and the Li density.

Ambient dose equivalent¹ (H*(10)) rate was assessed at contact and 1 m from the H-trap (at half height of the trap). ⁷Be and ACP decay gamma energies and intensities (Table 5) used in the simulations are from JENDL/DDF 2015 nuclear data library [12].

¹ H*(10) is the energy deposited by unit mass by an aligned and expanded radiation field in a point at 10 mm deep in the ICRU sphere (30 cm diameter and 1g/cm³ density).

Table 6
ACP activities and H*(10) rate (mSv/h) at contact and at 1 m from the trap for ⁷Be and dominant ACPs at half height of the H-trap in normal operation.

ACP	1 kg Y		3 kg Y		5 kg Y		8 kg Y	
	Activity Bq	1 m	Activity Bq	1 m	Activity Bq	1 m	Activity Bq	1 m
⁷ Be	1.50×10 ⁷	3.71×10 ⁻³	1.47×10 ⁷	3.50×10 ⁻³	1.44×10 ⁷	3.28×10 ⁻³	1.39×10 ⁷	2.97×10 ⁻³
⁵⁴ Mn	2.20×10 ⁸	9.00×10 ⁻¹	2.16×10 ⁸	8.61×10 ⁻¹	2.11×10 ⁸	8.20×10 ⁻¹	2.04×10 ⁸	7.59×10 ⁻¹
⁵¹ Cr	2.14×10 ⁵	3.19×10 ⁻⁴	2.09×10 ⁵	2.92×10 ⁻⁴	2.05×10 ⁵	2.67×10 ⁻⁴	1.98×10 ⁵	2.33×10 ⁻⁴
⁵⁷ Co	9.09×10 ⁸	2.23×10 ⁻¹	8.90×10 ⁸	1.54×10 ⁻¹	8.71×10 ⁸	1.14×10 ⁻¹	8.43×10 ⁸	8.02×10 ⁻²
⁶⁰ Co	6.48×10 ⁶	7.44×10 ⁻²	6.35×10 ⁶	7.15×10 ⁻²	6.22×10 ⁶	6.82×10 ⁻²	6.02×10 ⁶	6.40×10 ⁻²
^{60m} Co	4.29×10 ⁷	2.09×10 ⁻⁶	4.21×10 ⁷	9.71×10 ⁻⁷	4.12×10 ⁷	6.72×10 ⁻⁷	3.99×10 ⁷	4.77×10 ⁻⁷
⁵⁵ Co	2.81×10 ⁷	1.58×10 ⁻¹	2.75×10 ⁷	1.54×10 ⁻¹	2.69×10 ⁷	1.50×10 ⁻¹	2.61×10 ⁷	1.45×10 ⁻¹
⁵⁶ Co	3.65×10 ⁸	4.74	3.48×10 ⁸	4.63	3.41×10 ⁸	4.52	3.30×10 ⁸	4.37
⁵⁸ Co	1.19×10 ⁹	4.81	1.17×10 ⁹	4.68	1.14×10 ⁹	4.57	1.11×10 ⁹	4.41
⁵² Mn	3.10×10 ⁷	4.55×10 ⁻¹	3.03×10 ⁷	4.44×10 ⁻¹	2.97×10 ⁷	4.33×10 ⁻¹	2.88×10 ⁷	4.18×10 ⁻¹
⁵⁶ Mn	1.56×10 ⁸	1.18	1.53×10 ⁸	1.15	1.50×10 ⁸	1.13	1.45×10 ⁸	1.09
⁵⁷ Ni	2.24×10 ⁸	1.47	2.20×10 ⁸	1.43	2.15×10 ⁸	1.40	2.08×10 ⁸	1.35
¹⁸¹ W	3.22	2.2 × 10 ⁻¹⁴	3.15	1.8 × 10 ⁻¹³	3.08	1.5 × 10 ⁻¹³	2.99	1.3 × 10 ⁻¹³
²⁸ Al	1.4 × 10 ⁸	1.07	1.37×10 ⁸	1.05	1.34×10 ⁸	1.02	1.30×10 ⁸	9.89×10 ⁻¹
⁵² V	3.22×10 ⁶	3.70×10 ⁻²	5.63×10 ⁶	3.61×10 ⁻²	5.51×10 ⁶	3.53×10 ⁻²	5.33×10 ⁶	3.41×10 ⁻²
total		15.12		14.66		14.26		13.70
				0.296		0.299		0.279

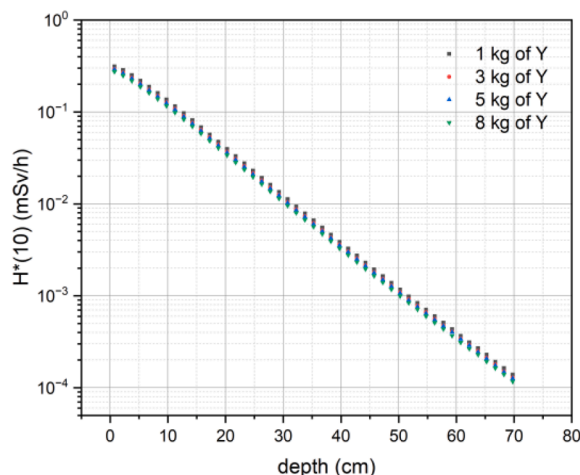


Fig. 3. H*(10) depth profile (in mSv/h) within a concrete wall located at 1 m of trap.

Ambient dose equivalents¹ per photon were calculated with radiation transport code MCNP 5.1.40 [13]. The code deals with transport of neutrons, gamma rays, and coupled transport, i.e., transport of secondary gamma rays resulting from neutron interactions. The MCNP code can also treat the transport of electrons, both primary source electrons and secondary electrons created in gamma-ray interactions. For photons, the code accounts for incoherent and coherent scattering, the possibility of fluorescent emission after photoelectric absorption, absorption in pair production with local emission of annihilation radiation, and bremsstrahlung. ICRP-74 flux to ambient dose equivalent factors [14] were implemented by using DE and DF cards in MCNP.

3. Results and discussion

3.1. Doses in normal operation

H*(10) rates obtained by Monte Carlo simulation during normal operation in contact with trap and 1 m from the trap at half height of the trap for the four different Y contents are shown in Table 6. Estimated activities of dominant ACPs has also been included in the table. Total H*(10) dose rate is in the range 13.7–15.1 mSv/h in contact and 0.28–0.31 mSv/h at 1 m from the trap. ⁵⁵Fe has a negligible contribution to dose due to the low energy of emitted gamma radiation. ⁷Be has a very low

contribution to H*(10) rate, between 3 and 3.7 μSv/h. ⁵⁸Co and ⁵⁶Co accounts for 63.2% of the dose. ⁵⁷Ni, ⁵⁶Mn, ²⁸Al and ⁵⁴Mn and ⁵²Mn contribute with 33.5% to total dose.

To know the effects in dose reduction of a concrete wall located at 1 m of the trap H*(10) rate was assessed as function of depth within concrete with MCNP. In order to reduce errors and computation time the variance reduction code ADVANTG [15] was used. Simulation was carried out for the ACP's that mainly contribute to dose (⁵⁸Co, ⁵⁶Co, ⁵⁷Ni, ⁵⁶Mn, ⁵⁴Mn and ²⁸Al). The results are shown in Fig. 3 for the four different Y contents considered. The half value layer (HVL) in concrete is 6.02 cm. Therefore a concrete wall 30 cm thick located at 1 m of the trap would reduce dose rate to the acceptable annual dose limits for workers (20 mSv/year or 10 μSv/h assuming 243 work days in a year).

3.2. Doses during maintenance

In maintenance operation the H-trap is emptied but a Li film remains attached to the Y pebbles. Maximum ⁷Be content attached to Y pebbles would occur in the case the H-trap is filled with 8 kg of Y and a Li film 100 μm thick. In that case ⁷Be mass present in the Li film would be 5.8×10^{-11} g assuming a ⁷Be concentration in Li of 1.052×10^{-7} apm which corresponds to a ⁷Be activity of 7.5×10^5 Bq. This value is quite below the exemption level, 10⁷ Bq [16]. Therefore, ⁷Be is not a matter of concern from the radiation protection point of view.

H*(10) rates obtained by simulation with MCNPX are presented in Table 7 for the four Y contents considered and the three Li film thickness. These are values in a point located at half height in contact with the trap. Estimated H*(10) rates are in the range 0.34–1.42 mSv/h in contact with the trap and 0.1–11 μSv/h at 1 m of the trap.

4. Conclusions

We have assessed the radiological impact of ⁷Be and other ACPs present in Li in the H-trap room of future IFMIF-DONES facility taking into account different Y contents in the trap during normal operation and maintenance. ⁷Be does not play an important role from the radiological point of view in normal operation and maintenance. In normal operation maximum H*(10) estimated by Monte Carlo radiation transport code MCNP is 15.1 mSv/h in contact with the H-trap and 0.31 mSv/h at 1 m from the trap. A concrete wall 30 cm thick located at 1 m of the trap would reduce dose rate to the levels acceptable for workers. In maintenance dose rates obtained with MCNP reveals maximum values of 1.42 mSv/h in contact with the trap and 11 μSv/h at 1 m of the trap.

Table 7

H*(10) dose rates (in μSv/h) in contact and 1 m from the trap during maintenance for 1, 3, 5 and 8 kg Y mass content and 10, 150 and 100 μm Li film thickness.

ACP	1 kg Y			3 kg Y			5 kg Y			8 kg Y		
	10 μm	50 μm	100 μm	10 μm	50 μm	100 μm	10 μm	50 μm	100 μm	10 μm	50 μm	100 μm
⁵⁴ Mn	2.02	10.57	21.77	5.32	26.73	52.82	7.63	37.47	72.69	9.98	48.04	90.80
⁵¹ Cr	6.1 × 10 ⁻⁵	3.2 × 10 ⁻⁴	6.8 × 10 ⁻⁴	1.5 × 10 ⁻⁴	7.8 × 10 ⁻⁴	1.6 × 10 ⁻³	2.1 × 10 ⁻⁴	1.0 × 10 ⁻³	2.1 × 10 ⁻³	2.6 × 10 ⁻⁴	1.3 × 10 ⁻³	2.5 × 10 ⁻³
⁵⁷ Co	0.22	1.24	2.70	0.44	2.28	4.67	0.50	2.55	5.08	0.52	2.61	5.20
⁶⁰ Co	0.17	0.89	1.82	0.45	2.26	4.44	0.65	3.20	6.15	0.86	4.14	7.79
^{60m} Co	1.2 × 10 ⁻⁶	6.5 × 10 ⁻⁶	1.4 × 10 ⁻⁶	1.6 × 10 ⁻⁶	8.0 × 10 ⁻⁶	1.6 × 10 ⁻⁵	1.7 × 10 ⁻⁶	8.4 × 10 ⁻⁶	1.6 × 10 ⁻⁵	1.7 × 10 ⁻⁵	8.4 × 10 ⁻⁶	1.6 × 10 ⁻⁵
⁵⁵ Co	0.36	1.86	3.83	0.94	4.72	9.29	1.35	6.64	12.81	1.78	8.53	16.09
⁵⁶ Co	10.89	56.11	115.25	28.72	143.34	281.31	41.52	203.03	390.37	54.93	262.57	493.94
⁵⁸ Co	10.80	56.39	116.25	28.38	142.71	281.89	40.64	200.06	387.62	53.15	255.89	483.94
⁵² Mn	1.04	5.39	9.02	2.73	13.68	26.91	3.94	19.31	37.20	5.18	24.84	46.85
⁵⁶ Mn	2.70	14.01	28.70	7.12	35.60	69.96	10.28	50.34	96.89	13.57	64.91	122.23
⁵⁷ Ni	3.39	17.53	35.76	8.94	44.57	87.37	12.94	63.21	121.42	17.17	81.97	148.81
¹⁸¹ W	2.5 × 10 ⁻¹³	1.4 × 10 ⁻¹²	3.0 × 10 ⁻¹²	5.2 × 10 ⁻¹³	2.7 × 10 ⁻¹²	5.6 × 10 ⁻¹²	6.3 × 10 ⁻¹³	3.2 × 10 ⁻¹²	6.43 × 10 ⁻¹²	6.86 × 10 ⁻¹³	3.43 × 10 ⁻¹²	6.8 × 10 ⁻¹²
²⁸ Al	2.50	12.87	26.21	6.59	32.79	64.17	9.57	46.66	89.45	12.75	60.71	113.95
⁵² V	0.09	0.44	0.90	0.23	1.13	2.21	0.07	1.60	3.07	0.44	2.08	3.90
total	34.10	177.30	336.00	83.27	417.01	820.87	119.52	587.41	1133.31	157.58	755.58	1419.55

CRedit authorship contribution statement

J. Javier Martínez-Serrano: Writing – original draft. **Yuefeng Qiu:** Supervision. **Tamás Dézsi:** Supervision, Methodology. **Francesco Sav-erio Nitti:** Supervision. **Angel Ibarra:** Supervision.

Declaration of competing interest

The authors declare that they have no known competing financial interests or personal relationships that could have appeared to influence the work reported in this paper.

Data availability

Data will be made available on request.

Acknowledgment

We want to thank Fernando Mota (CIEMAT) for his support in installing MCNP and ADVANTAG codes in parallel in XULA cluster. We thank Paolo Favuzza (ENEA), Eduardo Rodríguez and Jesús Castellanos for fruitful discussions.

References

- [1] S.P. Simakov, U. Fischer, and A.Y. Konobeyev. "Status and benchmarking of the deuteron induced Tritium and Beryllium-7 production cross sections in Lithium." *KIT Scientific Working Papers*; v. 147; 2020; 20 p; ISSN 2194-1629 (2020) 10 .5445/IR/1000120615.
- [2] Edao, et al., Tritium removal by Y hot trap for purification of IFMIF Li target, *Fusion Eng. Des.* 85 (2010) 53–57.
- [3] J.-C. Sublet, J.W. Eastwood, J.G. Morgan, M.R. Gilbert, M. Fleming, W. Arter, *FISPACT-II: an advanced simulation system for activation, transmutation and material modelling*, *Nucl. Data Sheets* 139 (2017) 77–137.
- [4] A.J. Koning, D. Rochman, J.C. Sublet, N. Dzysiuk, M. Fleming, S. van der Marck, *TENDL: complete Nuclear Data Library for Innovative Nuclear Science and Technology*, *Nucl. Data Sheets* 155 (2019) 1–55, <https://doi.org/10.1016/j.nds.2019.01.002>.
- [5] G. Bailey, D. Foster, P. Kanth, M. Gilbert, *The FISPACT-II user manual*, Culham Cent. 2 (2021). *Fusion Energy (CCFE)*. Culham. UK. Tech. Rep. UKAEA-CCFE-RE.
- [6] S.P. Simakov, U. Fischer, K. Kondo, P. Pereslavl'tsev, Status of the McDeLicious approach for the D-Li neutron source term modeling in IFMIF neutronics calculations, *Fusion Sci. Technol.* (2012) 233–239.
- [7] "FENDL-3.1d: fusion evaluated nuclear data library Ver.3.1d" <https://www-nds.iaea.org/fendl31d/>.
- [8] M. Frisoni, D. Bernardi, F.S. Nitti, Nuclear assessment of the IFMIF-DONES lithium target system, *Fusion Eng. Des.* 157 (March) (2020) 111658.
- [9] J. Castellanos, J. Molla, G. Barrera, S. Molla, Preliminary design of the H-trap, EUROFUSION IDM Report EFDA_D_2NEEJL. <https://idm.euro-fusion.org/?uid=2NEEJL>.
- [10] M. Ida, Estimation and control of beryllium-7 behavior in liquid lithium loop of IFMIF, *Fusion Eng. Des.* 82 (2007) 2490–2496.
- [11] R. Roman, Plant design description document of DONES, EUROFUSION IDM Report EFDA_D_2MP8HQ v2.1(2019) <https://idm.euro-fusion.org/?uid=2MP8HQ>.
- [12] J. Katakura and F. Minato. "JENDL decay data file 2015" "*JAEA-Data/Code 2015-030* (2016).
- [13] J.E. Sweezy, T.E. Booth, F.B. Brown, J.S. Bull, R.A. Forster III, J.T. Goorley, H.G. Hughes III, R.L. Martz, R.E. Prael, A. Sood, A.J. Zukaitis, R.C. Little, H.R. Trellue, M.C. White, M.B. Lee, S.M. Girard, MCNP - A General Monte Carlo N-Particle Transport Code, Version 5 - Volume 1: Overview and Theory. Los Alamos National Laboratory Tech. Rep. LA-UR-03-1987 (2003).
- [14] ICRP, Conversion Coefficients for use in Radiological Protection against External Radiation, ICRP Publication 74. *Ann. ICRP* 26 (1996) 3–4.
- [15] S.W. Mosher, et al., ADVANTG—An Automated Variance Reduction Parameter Generator, ORNL/TM 2013/416. Rev 1, Oak Ridge National Laboratory, 2015.
- [16] Council Directive 96/29/EURATOM, Laying down basic safety standards for the protection of the health of workers and the general public against the dangers arising from ionizing radiation (1996).